Lagrangian Coherent Structures

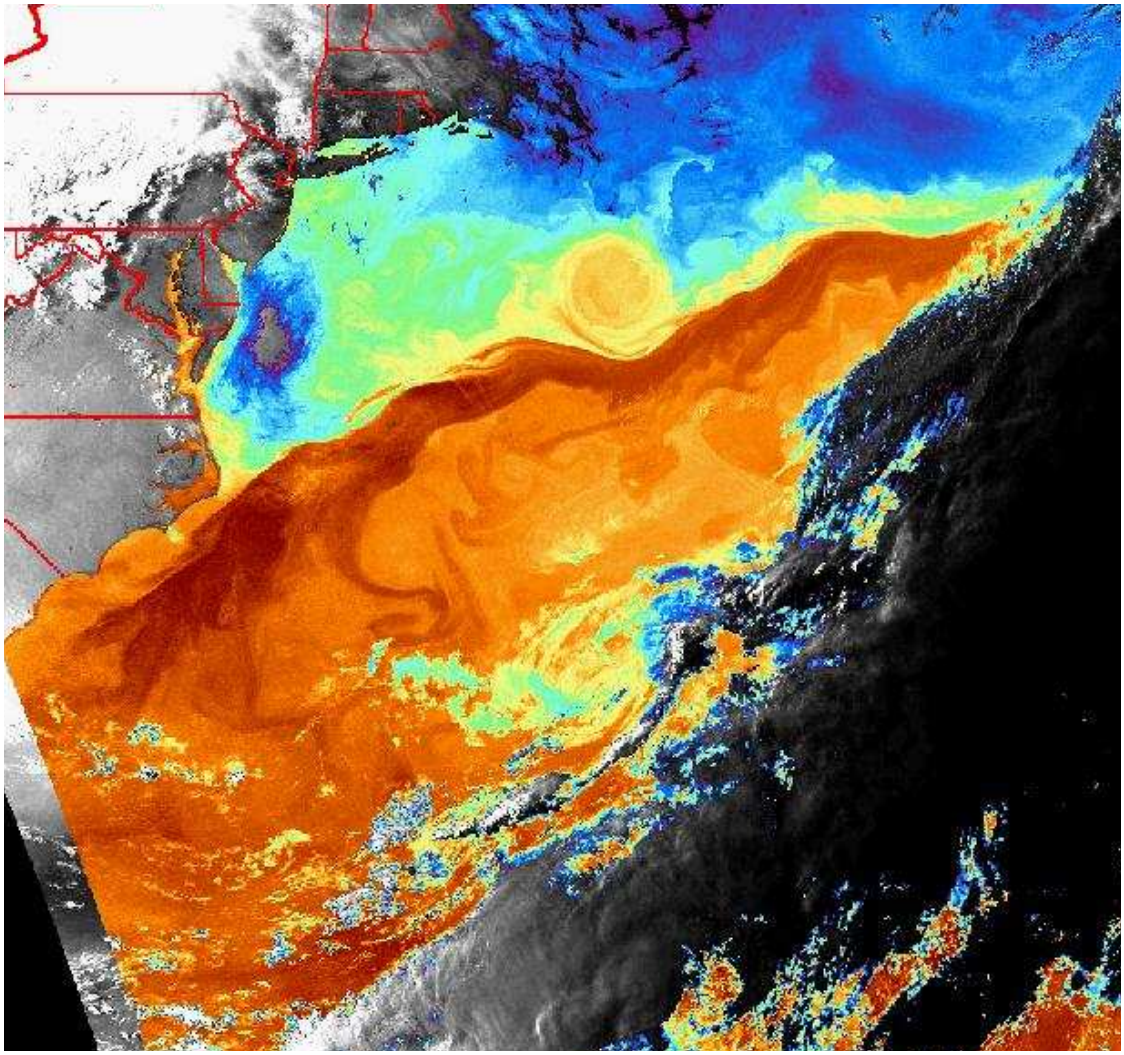

1 Eulerian versus Lagrangian approaches

The above figure is an AVHRR image of SST in the Gulf Stream region. Such images clearly demonstrate that there are coherent structures within the flow field that impact the distribution of tracers, in this case temperature, in producing thin filaments and ring-like features. The dispersion of the tracer is affected by strong stretching events which can lead to strong dispersion, and by features that block the transport of the tracer, so–called "transport barriers", such as at the edges of strong vortices. It would good to have a measure of the flow that indicates the transport and dispersive nature of the time–evolving flow field. One such measure in an Eulerian framework is the Okubo–Weiss parameter, W, (introduced by Okubo in 1970) given by

$$W = s_n^2 + s_s^2 - \zeta^2$$

where $s_n = u_x - v_y$ and $s_s = v_x + u_y$ are the normal and shear components of strain, respectively, and $\zeta = v_x - u_y$ the relative vorticity for a 2D flow field (u, v). In regions of the flow where $W \gg 0$ the flow is strain dominated while where $W \ll 0$ the flow is vorticity dominated. When applied to the identification of coherent eddies it is found typically that the inner core of the eddy which is vorticity dominated ($W \ll 0$) is surrounded by a region of strong strain ($W \gg 0$). The core edge is identified by a closed contour of $W = 0$. For a steady flow the core edge is a strong barrier to the exchange of a tracer between the core of the eddy and the exterior.

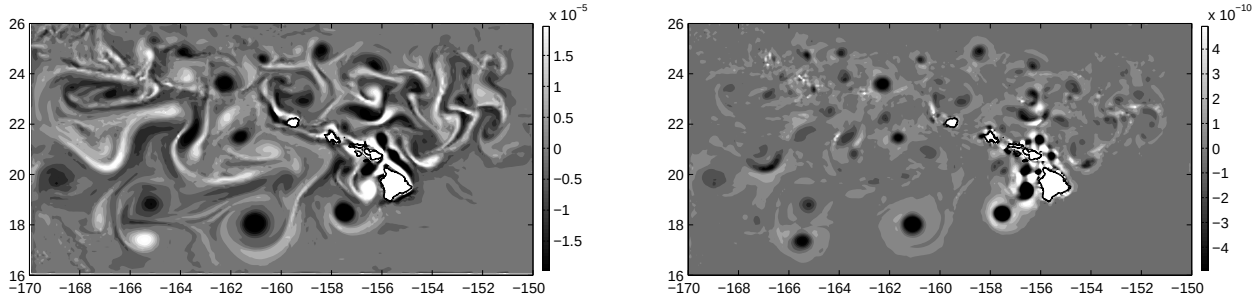

The above (taken from Calil et al, 2008) shows the relative vorticity field (left panel) and Okubo-Weiss parameter, W for a snap–shot of the flow from a regional model of the flow around the Hawaiian Islands. The vorticity field has strong cyclonic and anticyclonic eddies (intense white and black, respectively) interspersed by filamentary structures. The Okubo-Weiss parameter indicates the presence of strong eddies as intense black regions. Note that the eddy features, particularly those close to the islands, are surrounded by regions of strong strain.

The presence of the strong strain region surrounding eddies suggests that a small time dependence of the flow may affect the retentive nature of the eddy. Below is shown the dispersion of a tracer placed within the closed contours of the an eddy feature (taken from Lehahn et al, 2007).

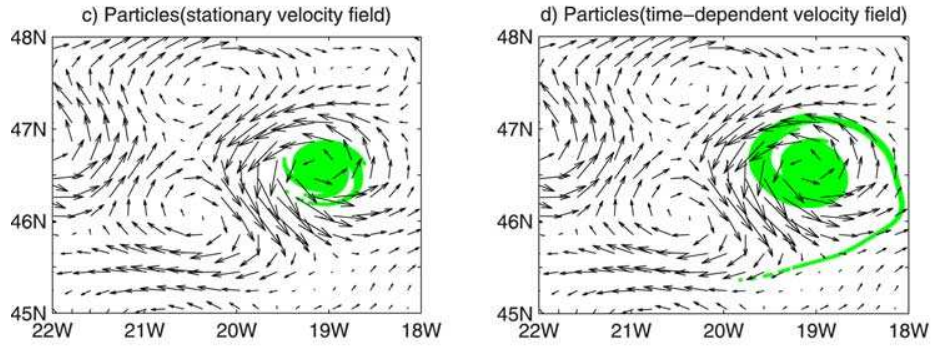

The tracer in the stationary flow field (left panel) remains contained within the eddy. In the non-stationary flow, however, a filament of tracer is drawn out indicating an exchange

of tracer across the edge of the eddy. Clearly, in a time evolving flow a Eulerian view has limitations in identify important features of the flow that affect tracer transport and dispersion. Tracer transport is an inherent Lagrangian property of the flow. We turn next to providing a Lagrangian framework in which to assess the properties of the flow.

2 Geometric concepts

2.1 Trajectories and phase space

Rather than describing the flow at a fixed point as a function of time, it can be instructive to consider the change in position of particles with time, the Lagrangian framework. The motion of a particle depends on the velocity, $\mathbf{v}$ at the location, $\mathbf{x}$ of the particle such that

$$\dot{\mathbf{x}} = \mathbf{v}(\mathbf{x}, t)$$

where $\mathbf{x} \in X$, X is $\mathbb{R}^2$ or $\mathbb{R}^3$, i.e. a 2 or 3 dimensional space, and t is time. The set X is known as the *phase space*. The solution $\mathbf{x}(t)$ for an initial condition $\mathbf{x}_o(t_o)$ describes a curve in the *phase space* referred to as an *orbit*, *particle path*, or *pathline* (the latter is used in the figure below: this and the next few figures are taken from lecture notes by George Haller)

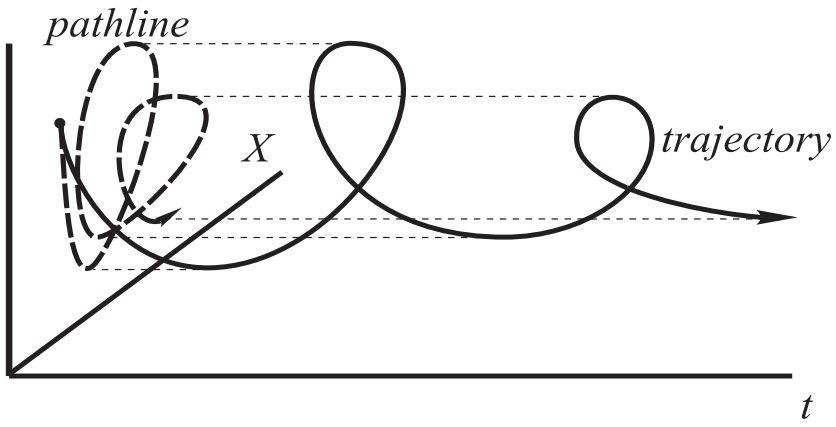

It is useful to extend the concept of a phase space to include the time axis, resulting in a space $X \times \mathbb{R}$ known as the *extended phase space* (see the figure above). A curve taken by a particle in this extended phase space is known as a *trajectory*. Note that while *pathlines* can intersect *trajectories* cannot.

2.2 Material surfaces/Invariant manifolds

We can define a surface in the extended phase space by considering a smooth set of trajectories that originate from a curve in the phase space X at a given time (see figure below). By definition, a trajectory originating on this surface always remains on the surface. The surface, M, in the extended phase space is known as *material surface*. In the terminology of dynamical systems this

is known as an *invariant manifold*, which in this case is two-dimensional. For a two dimensional flow field we can also construct invariant manifolds by considering a single trajectory or a surface which are one– and three–dimensional, respectively. In terms of the transport and dispersion of a tracer we would like to find those manifolds that significantly influence the character of the tracer transport, sometimes referred to as dynamically *distinguished*. These structures identify the *Lagrangian coherent structures* of the flow.

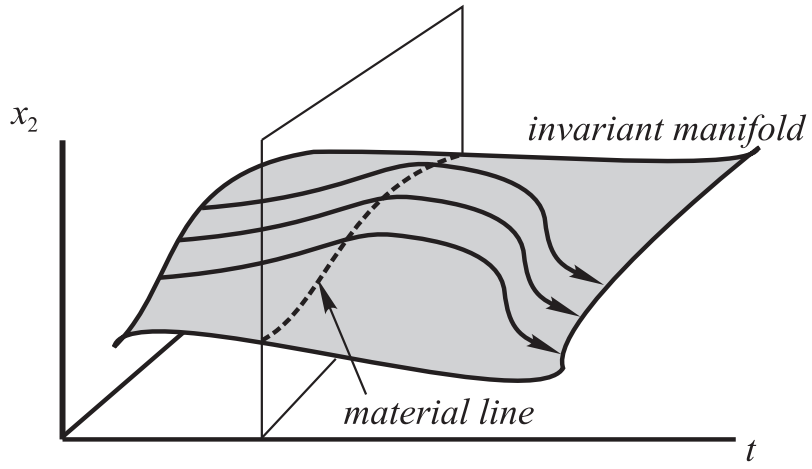

The behaviour of trajectories close to a given material surface can tell us lot about the dispersive character of the flow. Take the case shown below. Over the domain given by the dark shading on the material surface M the distance between M and adjacent trajectories grows (exponentially) with time. This can be viewed as the surface *repelling* trajectories that are close by. The material surface is said to be *unstable* over the given time interval. Alternatively, a material surface may be *stable* (*attracting*) over a some time interval.

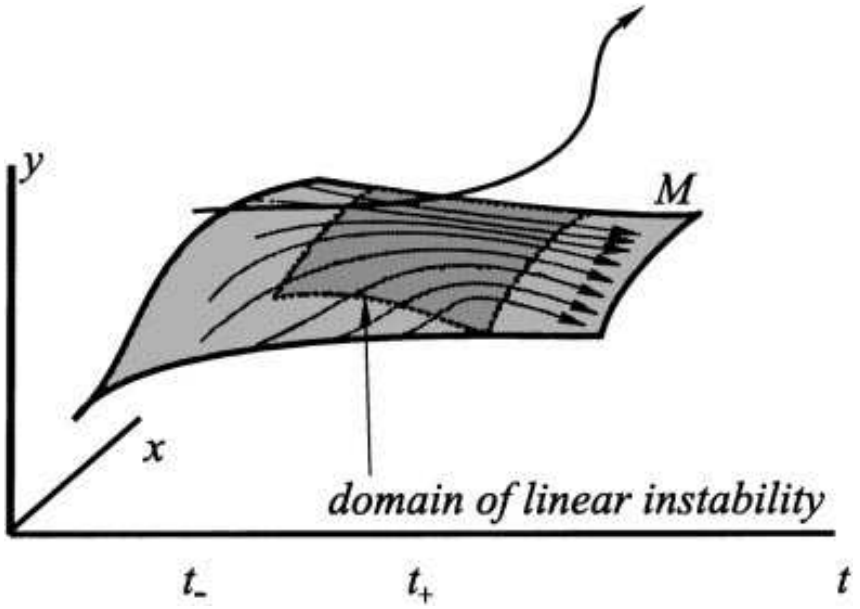

As a concrete example, and one that has very *distinguished* invariant manifolds, we consider a 2 dimensional steady plane strain flow in the (x_1, x_2) plane:

$$\mathbf{v} = A(x_1, -x_2)$$

where A is a constant. Particle paths in the (x_1, x_2) phase space are shown in (a) in the figure below.

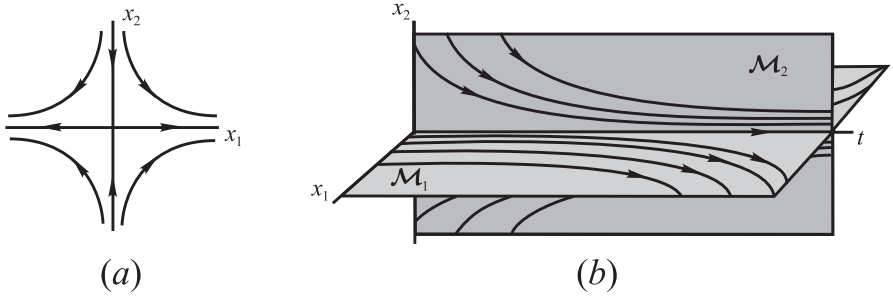

The flow has a saddle (*hyperbolic*) point at the origin. The invariant manifolds, M_1 and M_2, in the extended phase space, passing through the origin at $t = 0$, are shown in (b). M_1 and M_2 divide the flow into four distinct regions. A particle in one region remains in that region for all time. We also see that M_1 is a *stable* material surface while M_2 is an *unstable* material surface with nearby trajectories being *attracted* to and *repelled* from the two surfaces, respectively. Somewhat confusingly, the invariant manifolds M_1 and M_2 passing through the

hyperbolic point are known as the unstable and stable manifolds, respectively (i.e. opposite to the sense in which they act as material surfaces).

The trajectory of the hyperbolic point in the extended phase space is known the *hyperbolic trajectory*. In the case shown above the hyperbolic trajectory remains at $(0, 0) \, \forall \, t$. In general, the existence of the hyperbolic point may occur only for a limited time interval, or not at all, with the associated hyperbolic trajectory moving in the (x_1, x_2) plane.

The stable and unstable manifolds of the flow (whose existence and location will in general vary with time) and their intersection, particularly at hyperbolic points but also in other cases (see later), are therefore special properties of the flow that need consideration. In the vicinity of a stable manifold (unstable material surface) we expect strong dispersion. Unstable manifolds (stable material surfaces) not only act as attractors, they also can act as transport barriers. The impact of an unstable manifold on the distribution of a tracer field is shown in the figure below for a number of cases (figure taken from Lehahn et al, 2007).

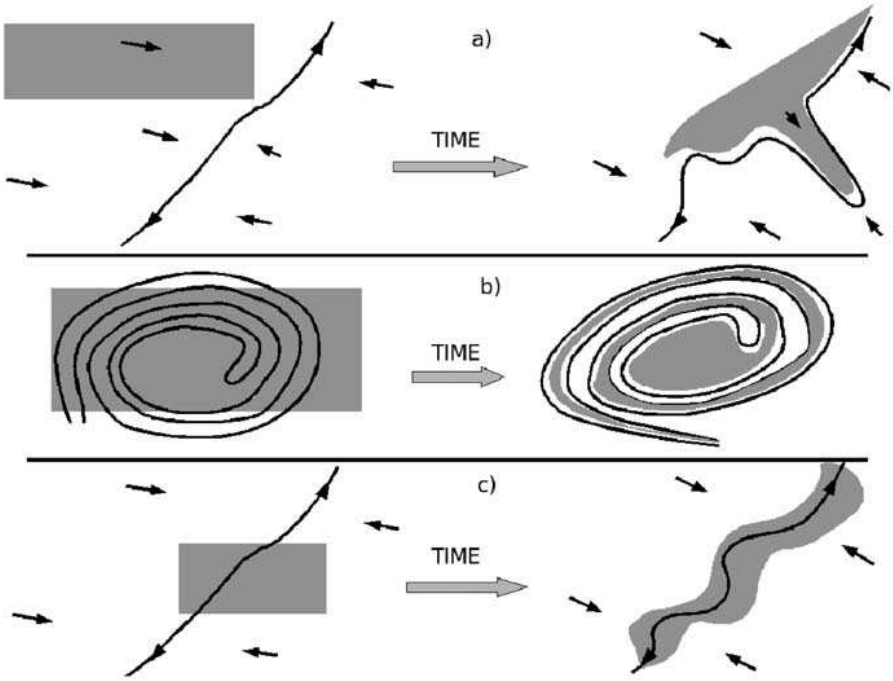

3 Detecting stable and unstable manifolds

Given their importance, a determination of the existence of *distinguished* invariant manifolds in a given flow seems desirable. A note of caution is needed here, however. The usefulness of these descriptors of the flow in assessing the impact the flow may have on a tracer distribution, or in interpreting model or observational results, will vary with the complexity of the flow field. The application of a dynamical systems approach to tracer transport and dispersion in fluids is a relatively new research area. To date the most useful applications have been in cases where there are distinct structures in the flow field. In more complicated cases their worth is less

clear. Future developments in flow descriptors and their application may well extend the range of useful applicability of such techniques.

Unfortunately, except in simple cases such as that above, it is not possible to provide an analytic expression for the stable and unstable manifolds of a flow. We therefore have to resort to numerical methods. A number of techniques have been developed, although it should be stressed there is at present no rigorous basis for any of them. Here we consider one particular technique that has proved popular in recent years, namely the use of finite size Lyapunov exponents (FSLEs).

3.1 Finite Size Lyapunov Exponents

The dispersion of tracers can be characterized by the rate at which two particles, which are initially close together, separate. As suggested by the figure below particle pairs that originate close to a stable manifold will quickly separate (exponentially)if the flow is integrated forward in time. Alternatively, if the flow is integrated backwards in time it is particles placed close to the unstable manifold that will separate exponentially.

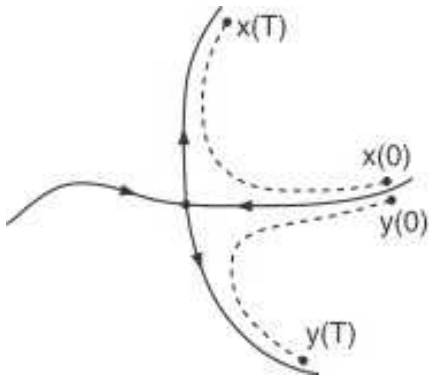

The Lyapunov exponent, $\lambda(\mathbf{x}, t)$, which gives a measure of the separation rate for an infinitesimal initial separation, is defined by

$$\lambda(\mathbf{x}, t) = \lim_{T\to\infty} \lim_{\delta(\mathbf{x},t,0)\to 0} \frac{1}{T} \ln \frac{\delta(\mathbf{x}, t, T)}{\delta(\mathbf{x}, t, 0)}$$

where $\delta(\mathbf{x}, t, T)$ is the separation at time $t + T$ for a pair initially centered on $\mathbf{x}$ at time t. For a statistically spatially and temporally heterogeneous flow the limit $T \to \infty$ is not useful, while for a domain that is well mixed at large times λ is uniform over the domain giving no information about the Lagrangian structures within the flow.

Rather than deal with an infinitesimal separation, and infinite time, we consider instead a finite initial separation and a finite final separation. The finite-size Lyapunov exponent (FSLE) is defined as

$$\mu(\mathbf{x}, t, \delta_0, r) = \frac{1}{\tau} \ln r$$

where τ is the time it takes for the separation to increase to $\delta(\mathbf{x}, t, \tau) = r\delta_0$ (c.f. Aurell et al 1997, Artale et al 1997, Joseph and Legras 2002). The resolution δ_0 is limited by the need for the separation to increase to the desired scale (e.g. the integral length scale of the eddies) by an appropriate time (e.g. the integral time scale).

In practice the *forward* FSLE is calculated by seeding the flow with a large large of particles on a regular grid. The FLSE, μ, is then calculated from the time it takes for the initial separation to increase by the factor r, and the value for μ is mapped back to the mid–point of the initial position of the particle pair. In order to avoid the dependence on the orientation of the pairs of particles, the FSLE is obtained by diagonalizing the linear transformation of a square whose diagonals are formed by two pairs of particles. The expectation is that ridges of high values of μ will approximately coincide with the *stable* manifolds in the flow. The *unstable* manifolds can be detected by the *backward* FSLEs which are calculated by integrating backwards in time.

To demonstrate that FSLEs are effective at detecting unstable manifolds the figures below compare the unstable manifold of the forced Duffing equation, which can calculated very accurately by numerical means, and the FSLE for the same flow (from Joseph and Legras, 2002). There is a good correspondence between the two and suggests the FSLE is able to capture much of the detail of the unstable manifold.

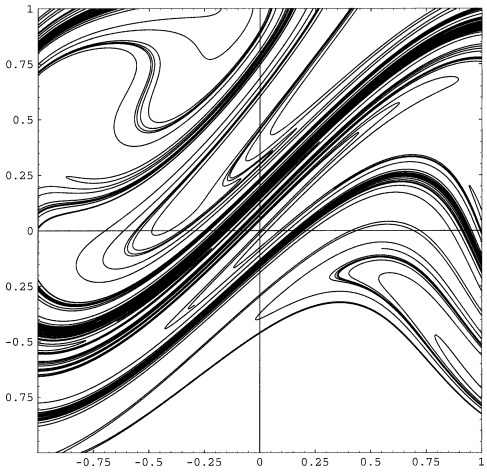

FIG. A3. The unstable manifold of the forced Duffing equation in a rotating frame plotted at time $t = 0$. See the text for the construction of this figure.

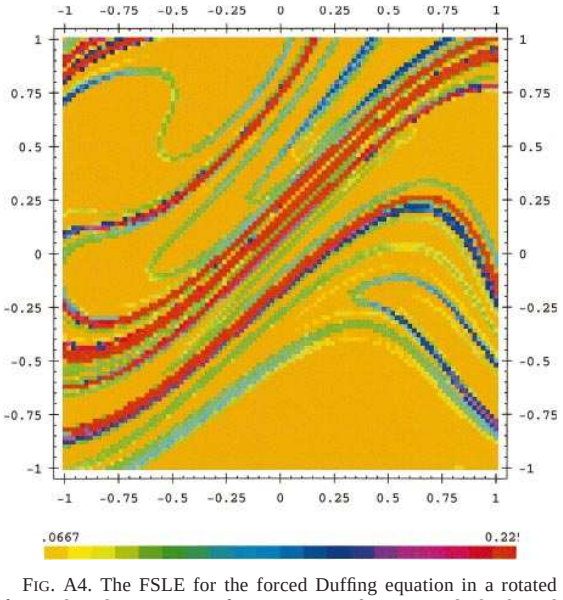

FIG. A4. The FSLE for the forced Duffing equation in a rotated frame plotted at time $t = 0$ for a separation $\delta\mathbf{x} = 1.5$ and a backward integration time $T = 15$. Values are as indicated in the caption.

The stable and unstable manifolds, determined by calculating the FSLEs, for the polar vortex in the Southern Hemisphere in October 1996 are shown below superimposed on the PV. Most notable is the filament of PV which has been ejected from a point coinciding with the crossing of the stable and unstable manifolds at O_1 and aligned with one branch of the unstable manifold (from Joseph and Legras, 2002). This strongly suggests the presence of an hyperbolic point at O_1. Although less obvious, the point O_2 is also likely to be a hyperbolic point, as determined by the release of tracers in its vicinity.

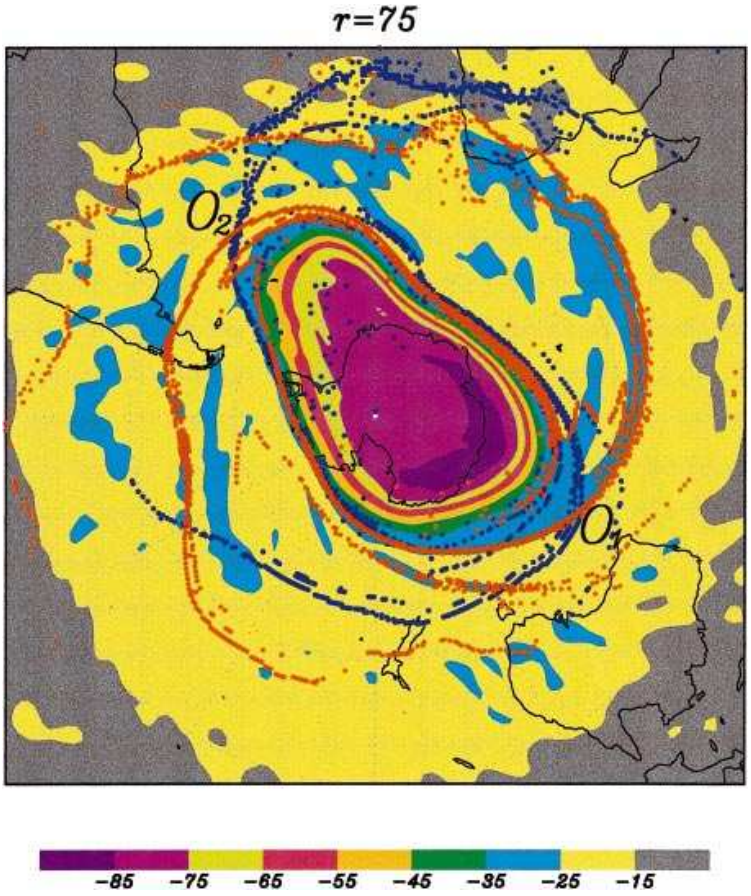

FIG. 2. Contours: potential vorticity map at 1200 UTC 25 Oct 1996 and on the isentropic level $\theta = 500$ K from the T106/L15 spectral analysis of ECMWF. Color scale is in PV units (PVUs) (1 PVU = 10^{-6} K kg^{-1} m^2 s^{-1}). Dots: initial locations of pairs that have grown their separation by a factor $r = 75$ within 9 days; red: backward integration (unstable manifold); blue: forward integration (stable manifold).

Close to the point O_2 there are a number of intersections of the stable and unstable manifold producing two *lobes*. Such lobes are known to be important in the exchange of fluid between the interior and exterior of the vortex, creating something called the *turnstile* effect. Estimating the area of each lobe gives the ratio of the fluid ejected to that entrained into the vortex.

As an oceanographic example we show the stable and unstable manifolds of a flow field in the N Atlantic calculated by Lehahn et al (2007). Here the velocity field is the geostrophic velocity estimated from the surface height field measured by satellite. A green patch of tracer was released close to the hyperbolic point in the center of the figure and its subsequent evolution calculated by numerically integrating forward in time using the observed flow field. Six days later the tracer has collapsed onto the unstable manifold. A patch of chlorophyll observed from the ocean colour is aligned along the same unstable manifold, and a filament in the SST field is aligned along its extension.

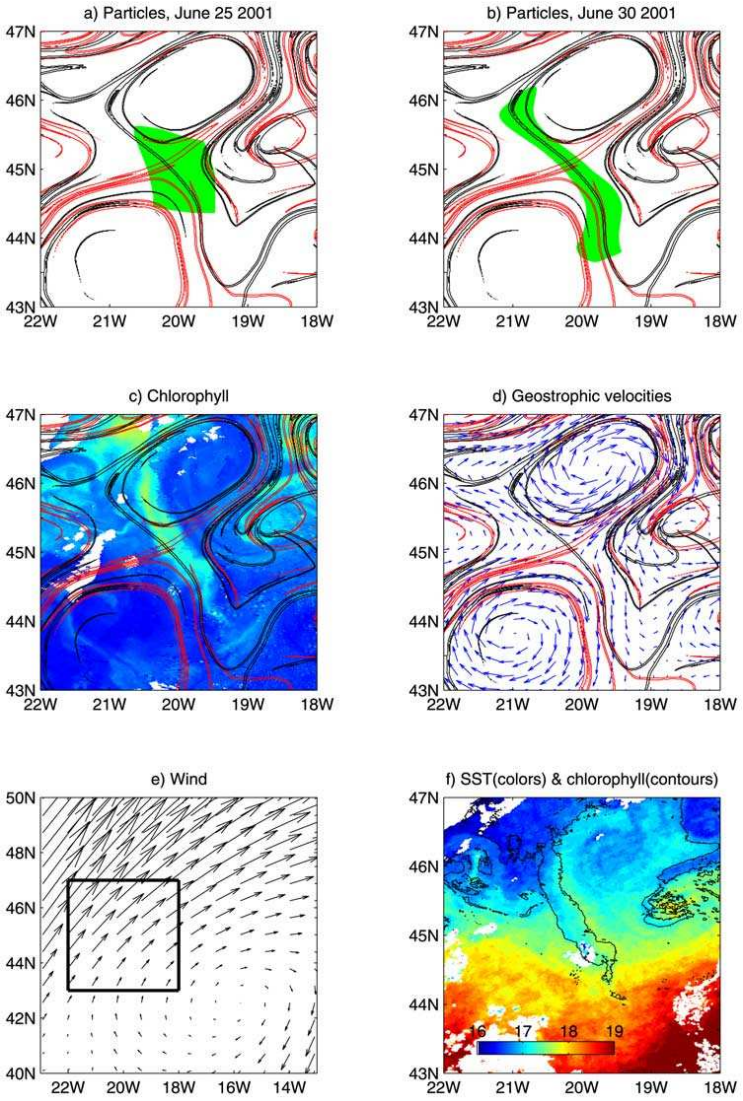

Figure 11. (a, b) Time evolution of synthetic passive particles (green dots) advected by the geostrophic velocity field. The particles are initiated on 24 June 2001 as a patch around the hyperbolic point at 20°W/ 45°N; (c) chlorophyll (colors, same scale as in Figure 7f); (d) geostrophic velocity field (arrows); (e) wind stress (arrows, the frame marks the boundaries of the other images in this figure); and (f) superposition of chlorophyll (contours) and SST (colors). The data are from 30 June 2001. The red and black lines correspond respectively to the strong stable and unstable manifolds.

Here δ_0 was taken as 0.01° ($\sim$ 1km) and $r = 80$ (i.e. a final separation of $\sim$ 80km). Note that although the velocity is relatively smooth the hyperbolic manifolds are sharp and well defined.

The final example uses the same technique for the flow around the Hawaiian Islands (only the unstable manifolds are shown)

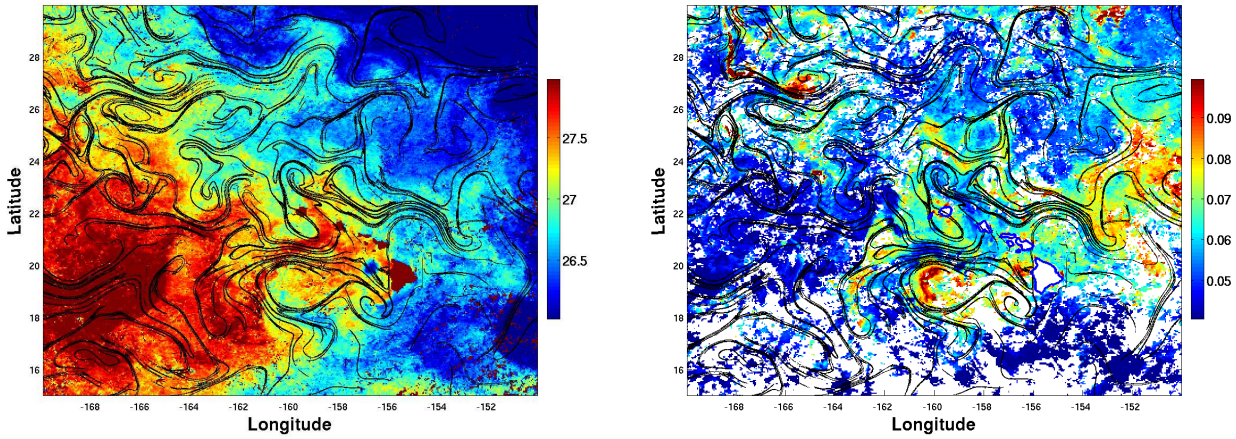

October 1–7 2004: (a) SST (color) with FSLE's superimposed (black lines); (b) Surface chlorophyll concentration (color) with FSLE's superimposed (black lines).

Although there some notable exceptions, a number of the features in the SST and chlorophyll distributions are aligned along unstable manifolds.

4 Association of vertical motions and Lagrangian coherent structures

As well as affecting the lateral transport and stirring of tracers Lagrangian coherent structures, in particular hyperbolic trajectories, can also be associated with regions of strong vertical motions. This is particularly important for primary production which can respond to the associated flux of nutrients (implied in the work of Lehahn et al 2007). As an example we show results from a regional ocean model for the flow around Hawaii (Calil and Richards, in prep). Note that strong gradients in surface density are often associated with an unstable manifold (indicated by the backward FSLE). These strong density gradients (fronts) are also associated with regions of large vertical velocity.

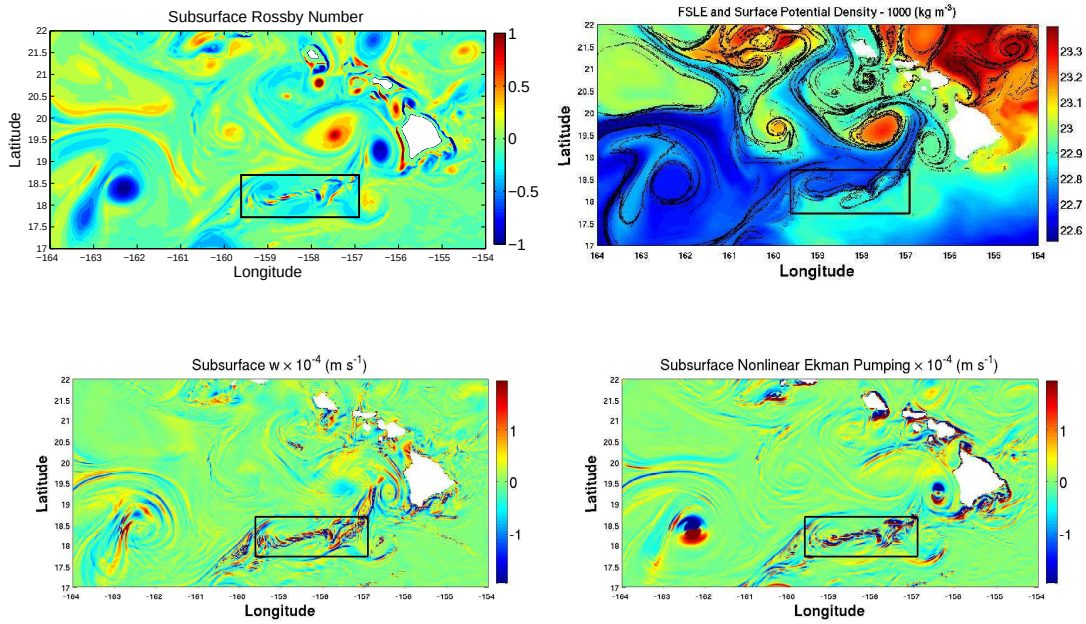

(a) Subsurface Rossby number, (b) FSLEs superimposed on surface potential density, (c) subsurface vertical velocity, w, (d) nonlinear Ekman pumping velocity, w_{nl}.

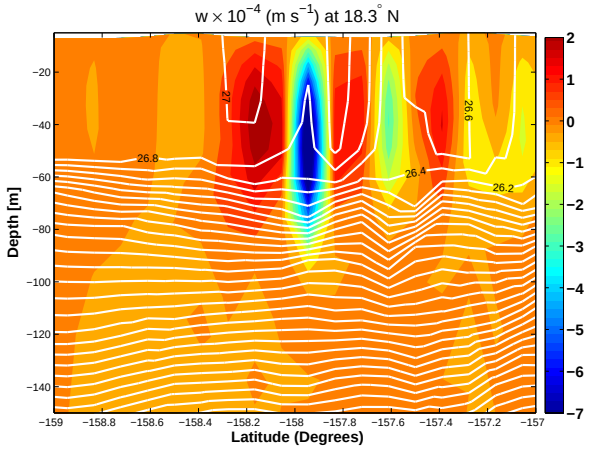

Cross frontal section of vertical velocity and potential temperature

Here we briefly describe two mechanisms that induce large vertical velocities. See Thomas et al (2008) for a review of recent work in this area.

4.1 Strain-Driven Frontogenesis

Strain-driven frontogenesis is a consequence of the enhancement of horizontal density gradients caused by the deformation of the geostrophic field. A strong straining of the flow, such as associated with a hyperbolic trajectory (see below), tends to sharpen lateral gradients of properties.

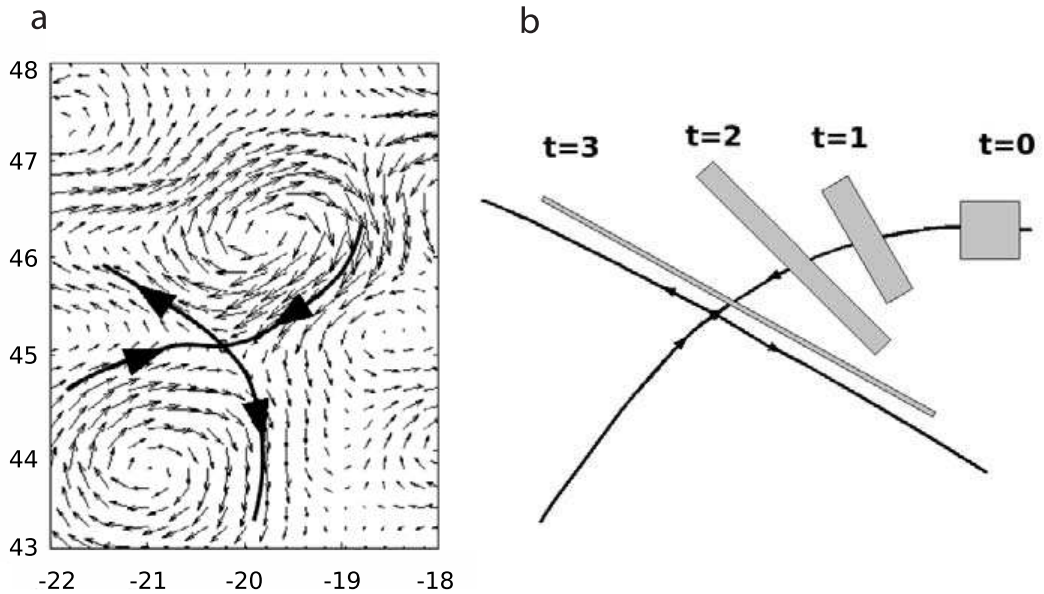

In the case of density this has dynamical consequences. The flow is taken out of thermal wind balance (the vertical shear in velocity no longer balances the lateral gradient in density). To compensate, counter-rotating, ageostrophic, cells are generated that produce a slumping of the density front and a tendency to reestablish a geostrophic balance (Hakim et al, 2002: Lapeyre and Klein, 2006; Legal et al, 2007).

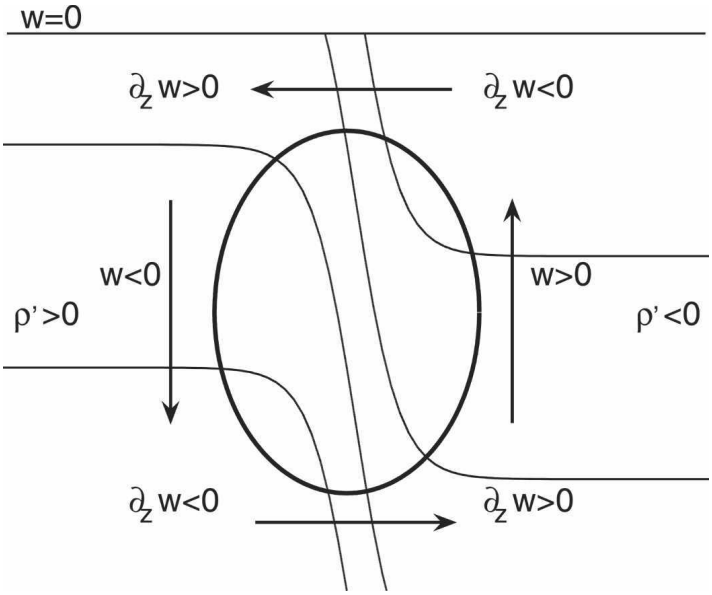

4.2 Nonlinear Ekman Pumping

When the local Rossby number is O(1) (see figure above), the nonlinear terms in the momentum equation become important and can no longer be ignored when deriving the vertical velocity induced at the base of the Ekman layer by the wind forcing (Thomas and Rhines, 2002). The *non-linear* Ekman pumping is given by

$$w_{nl} = \frac{\partial}{\partial x}\left[\frac{\tau^y}{\rho_0(f+\zeta)}\right] - \frac{\partial}{\partial y}\left[\frac{\tau^x}{\rho_0(f+\zeta)}\right]. \tag{1}$$

Note that in this case even a uniform wind induces vertical velocities provided that the gradients of the geostrophic relative vorticity, ζ, are strong. Gradients of relative vorticity are pronounced in regions of strong stretching, detected by the (backward) FSLE, and we may expect to find large vertical velocities induced by nonlinear Ekman pumping (see above). Note also that the nonlinear Ekman pumping may act constructively or destructively with the ageostrophic motions induced by frontogenesis, depending on the direction of the wind.

References

Artale, V., G. Boffetta, A. Celani, M. Cencini, and A. Vulpiani, Dispersion of passive tracers in closed basins: Beyond the diffusion coefficient, *Phys. Fluids*, **9**, 3162–3171, 1997.

Aurell E., G. Boffetta, A. Crisanti, G. Paladin, and A. Vulpani, Predictability in the large: An extension of the concept of Lyapunov exponent, *J. Phys, A: Math. Gen.*, **30**, 1-26, 1997.

Calil, P. H. R., K. J. Richards, Y. Jia, and R. Bidigare, Eddy activity in the lee of the Hawaiian Islands, *Deep-Sea Research II*, doi:10.1016/j.dsr2.2008.01.008, 2008.

Hakim, G., C. Snyder, and D. Muraki, A New Surface Model for Cyclone–Anticyclone Asymmetry, *Journal of the Atmospheric Sciences*, 59(16), 2405–2420, 2002.

Haller, G., and G. Yuan, Lagrangian coherent structures and mixing in two–dimensional turbulence, *Physica D*, **147**, 352–370, 2000.

Joseph B., and B. Legras, Relation between kinematic boundaries, stirring, and barriers for the Antartic polar vortex, *J. Atmos. Sci.*, **59**, 1198–1212, 2002.

Lapeyre, G., and P. Klein, Impact of small-scale filaments on the oceanic vertical pump, *J. Mar. Res.*, **64**, 835–851, 2006.

Legal, C., P. Klein, A. Treguier, and J. Paillet, Diagnosis of the Vertical Motions in a Mesoscale Stirring Region, *Journal of Physical Oceanography*, **37**(5), 1413–1424, 2007.

Lehahn, Y., F. d'Ovidio, M. Lévy, and E. Heifetz, Stirring of the northeast Atlantic spring bloom: A Lagrangian analysis based on multisatellite data, *Journal of Geophysical Research*, **112**, doi:10.1029/2006JC003927, 2007.

Thomas, L., and P. Rhines, Nonlinear stratified spin-up, *Journal of Fluid Mechanics*, **473**, 211–244, 2002.

Thomas, L., A. Tandon, and A. Mahadevan, Submesoscale processes and dynamics, submitted *J. Geophys. Res.*, available from http://varun.bu.edu/.